Alternative to classic annealing treatments for fractally patterned TiO$_2$ thin films

O. Van Overschelde,[1,a)] G. Guisbiers,[2] F. Hamadi,[3] A. Hemberg,[4] R. Snyders,[4,5] and M. Wautelet[1]

[1]*Physics of Condensed Matter, University of Mons-Hainaut, Avenue Maistriau 23, 7000 Mons, Belgium*
[2]*CICECO, Campus Santiago, University of Aveiro, 3810-193 Aveiro, Portugal*
[3]*Advanced Technologies Development Centre (CDTA), P.O. Box 17, Baba-Hassen Algiers, Algeria*
[4]*Inorganic and Analytical Chemistry, University of Mons-Hainaut, 1 Avenue Copernic, 7000 Mons, Belgium*
[5]*Materials Chemistry, RWTH Aachen University, 16 Kopernikusstrasse, 52074 Aachen, Germany*

Titanium dioxide thin films have been deposited by reactive magnetron sputtering on glass and subsequently irradiated by UV radiation using a KrF excimer laser. The influence of the laser fluence (F) on the constitution and microstructure of the deposited films is studied for $0.05 < F < 0.40$ J/cm^2. The diffraction data reveal that as deposited films are amorphous, while irradiated films present an anatase structure. Additional Raman spectroscopy study shows better crystal quality for the films irradiated with $F < 0.13$ J/cm^2. The film morphology appears to be strongly modified after laser treatment. Atomic force microscopy and scanning electron microscopy measurements reveal fractally textured films presenting characteristics of high porosity and high specific surface area. Finally, contact angle analysis suggests hydrophobic or wetting behavior depending on F. In order to explain the laser-induced structuration mechanisms, we have successfully applied a fractal as well as the nucleation theories. We propose that electronics effects could be responsible for the observed crystallization. © 2008 American Institute of Physics. [DOI: 10.1063/1.3021161]

I. INTRODUCTION

In the semiconductor technology, laser-induced crystallization is used because it presents selective optical absorption and low processing temperature[1] TiO$_2$ presents three polymorphous structures, namely, anatase (a-TiO$_2$), rutile (r-TiO$_2$), and brookite (b-TiO$_2$). On a technological point of view, a-TiO$_2$ presents a lot of interest because of its excellent photocatalytic behavior.[2] Indeed, a-TiO$_2$ is expected to be the most common photocatalyst for pollutant degradation due to its chemical stability and low toxicity.[3] The conventional deposition techniques of a-TiO$_2$ such as magnetron sputtering[4,5] lead most of the time to a relatively smooth film, which is not the optimal morphology for photocatalyic applications. Therefore, new strategies to synthesize morphologically adapted a-TiO$_2$ thin films for photocatalytic applications are of great importance. Postannealing treatment has been often used to crystallize Au/Ge bilayer films where topography of metal Au film appeared to play a major role in nucleation process.[6,7] In the same way, initially amorphous TiO$_2$ were postannealed in order to modify topography and crystallographic constitution.[8,9] Unfortunately, the a-TiO$_2$, obtained by classic annealing methods (taking minutes to hours to obtain transformations[10]), in comparison to r-TiO$_2$, is more difficult to synthesize because it is thermodynamically less stable.[4] Therefore, efforts still have to be realized to optimize the microstructure of a-TiO$_2$ thin films by laser irradiation methods. It has been shown that excimer laser is a powerful technique to process the surface after deposition;[11,12] for instance, laser treatment of SnO$_2$ thin films appeared to be an interesting technique to produce porosity and high surface area, which are desirable for gas sensor design.[13] Excimer laser interaction with TiO$_2$ thin films can be described by four main regimes depending on the laser fluence.[14,15] At low F (<0.075 J/cm^2), no transformation takes place, as supported by x-ray diffraction experiments and profilometry measurements. Increasing F, for $F \sim 0.075$ J/cm^2, x-ray diffraction data suggest a crystallization of the initially amorphous film into a-TiO$_2$. When F increases further, the morphology of the film is observed as a fractal structure. The fractal nature of the topography will be described by means of fractal dimension, seeing that the concept of fractal geometry has proved useful in describing structures and processes in experimental systems.[16] When F reaches a value of 0.8 J/cm^2, ablation takes place.[12] The interesting range of fluence is the one where crystallization is observed; thus, we restrict ourselves to that domain, namely, $0.075 < F < 0.35$ J/cm^2. We report on the quality of a-TiO$_2$ and the surface morphology generated by excimer laser irradiation.

II. EXPERIMENTAL DETAILS

TiO$_2$ films are deposited by reactive magnetron sputtering in an Ar/O$_2$ mixture. The deposition chamber consists of an industrial system (TSD 400-CD HEF R&D). Titanium target (99.9% purity) with an area of 45×15 cm^2 and a thickness of 0.8 cm is sputtered in dc mode using an ENI RPG 100 generator. The maximum power is 10 kW with a

---

a)Author to whom correspondence should be addressed. Electronic mail: olivier.vanoverschelde@umh.ac.be.

104, 103106-1

maximum voltage of 800 V. 208 nm thick TiO_2 coatings are deposited on 180 cm^2 glass substrate. No intentional heating of the substrate is performed.

After deposition, the films are irradiated in air using a Lambda Physik (Model Compex 205) excimer laser (248 nm wavelength, 25 ns pulse duration). The laser fluence is modified by varying the distance between an UV lens (250 mm focal length) and the sample. TiO_2 thin films are crystallized by single shot excimer laser annealing at different laser energy densities.

Thickness and roughness (average values calculated from three different positions on the sample) of the irradiated films are evaluated by means of a DEKTAK 3030ST profilometer. Three dimensional surface profiles are measured by atomic force microscopy (AFM) by using a Veeco Nanoscope III—a microscope (300 kHz tapping mode). From these last measurements, roughness and fractal measurements are carried out using WSXM software.[17] The coating's microstructure characterization is also performed with scanning electron microscopy (SEM) (Hitachi SU-70).

The crystallization of the TiO_2 films is examined by x-ray diffraction using a D8 Discover goniometer equipped with HI-STAR 1024×1024 pixels two-dimensional (2D) detector (Bruker-AXS Inc.). Cu source is used with acceleration voltage and current of 40 kV and 40 mA, respectively. The detector to sample distance is 15 cm. The goniometer is equipped with pinhole collimator, laser, and camera for focusing on the area of the sample to be measured. The incident angle is 5° with frame width of 32° and measurement time 120/240 s/frame. The Raman spectra acquisition is done with the Horiba Jobin Yvon LabRAM HR 800 UV with a laser light emission at 325 nm.

The lowest fluence irradiation samples are analyzed with a Horiba Jobin Yvon MM-16 spectroscopic ellipsometer. The analysis of these measurements is performed with the DELTAPSI2™ software. The irradiated surface's wettability is determined with a drop of water using a GBX DIGIDROP contact angle meter.

III. EXPERIMENTAL RESULTS

A. Crystallographic constitution

The as deposited films appear to be amorphous as shown by x-ray diffraction. Figure 1 shows the evolution of the intensity of the (101) anatase diffraction peak (I_{101}) with increasing F. No rutile phase is detected. At low F (<0.075 J/cm^2), the irradiated film remains amorphous. The anatase phase increases with increasing F up to a maximum, around $F=0.13$ J/cm^2, and then decreases linearly with F. This last behavior could be associated to a decrease in the material quantity. Indeed, although we are below the ablation threshold, vaporization could appear in low energy laser processes.[18] No diffraction peak is detected for $F \geq 0.35$ J/cm^2.[19]

Laser-induced crystallization appears in this case in a short range of low F. This F-range, where crystallization is observed, is known to be an "inflating" regime.[11] In order to get more details on the crystallographic constitution of the film, Raman spectroscopy has been performed. Raman spec-
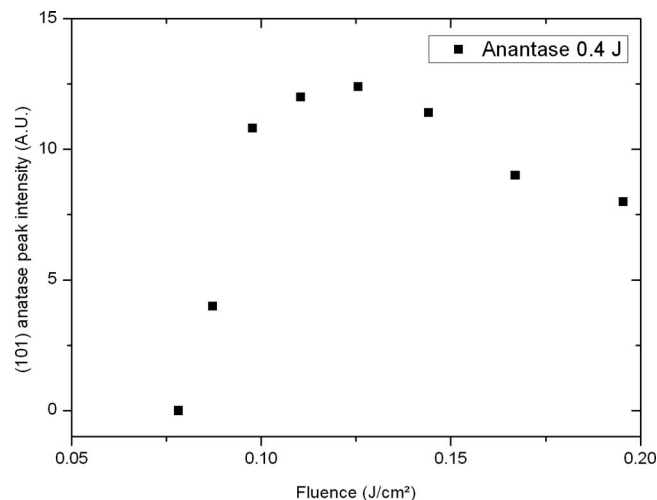

FIG. 1. Evolution of the (101) anatase diffraction peak as a function of the laser fluence.

tra are shown on Fig. 2. The most intense Raman mode observed is ~639 cm^{-1} corresponding to a-TiO_2.[20] These data support our x-ray diffraction measurements. Surprisingly, the as deposited film shows a Raman spectrum although no diffraction peak has been observed on the diffraction pattern. This could be explained by the fact that Raman technique is also sensitive to amorphous phases.[21]

In order to estimate the crystal quality, we have fitted the three main Raman peaks observed in a spectrum, namely, 1, 2, and 3 (Fig. 2), with a Lorentzian function to measure the full width at half maximum (FWHM). The variation in FWHM with F is shown in Fig. 3. It appears that the peaks are thinner than the nonirradiated sample for $F < 0.13$ J/cm^2 and larger when $F > 0.13$ J/cm^2. From these last observations, we could deduce that the crystal quality is better in that F range.

B. SEM and ellipsometry measurements

After laser irradiation, the surface texture is more or less modified depending on F. Figure 4 shows a top view SEM picture of (a) an as deposited film and (b) an irradiated one
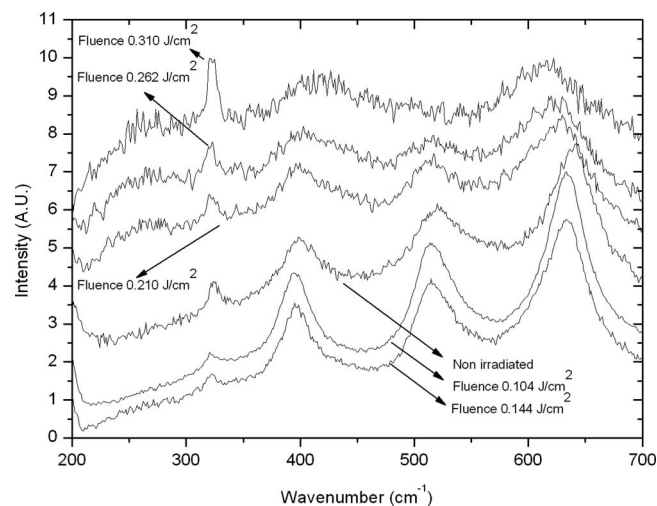

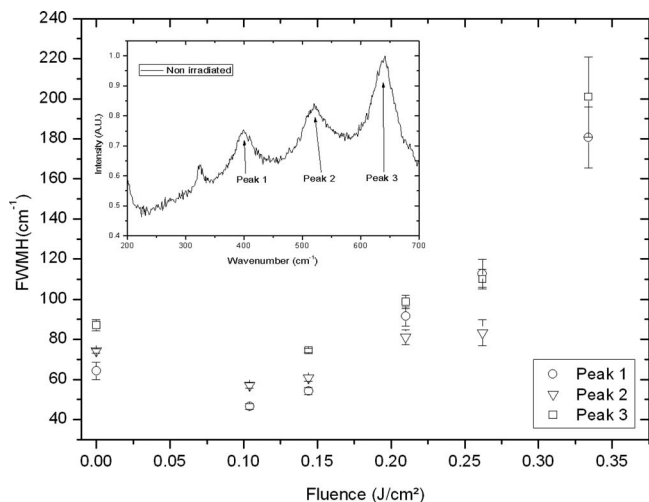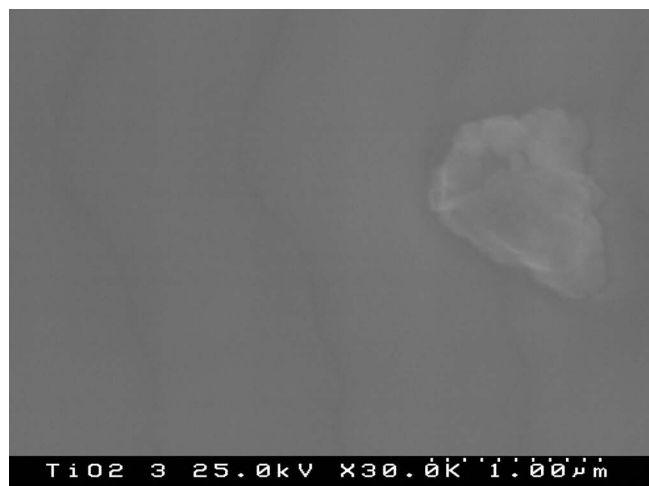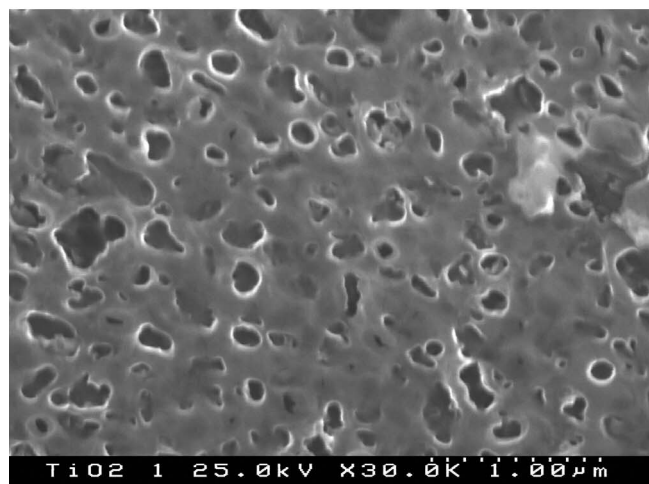FIG. 2. Raman spectra of irradiated TiO_2 for various fluences

FIG. 3. Evolution of FWHM function of fluence.

FIG. 5. (3×3 μm^2) three-dimensional AFM images of irradiated TiO_2 thin film for fluence (a) 0.09 J/cm^2, (b) 0.12 J/cm^2, (c) 0.14 J/cm^2, (d) 0.19 J/cm^2, (e) 0.25 J/cm^2, and (f) 0.3 J/cm^2. (g) as deposited TiO_2.
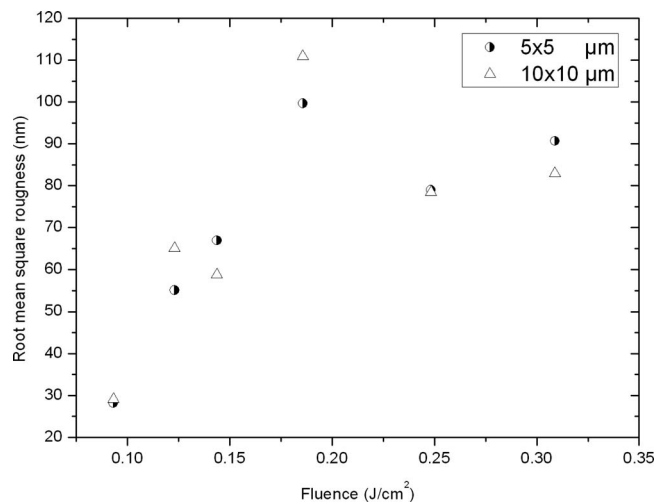
who appears porous. This porous morphology is confirmed by spectroscopic ellipsometry analysis. This last technique reveals, for a wavelength of 450 nm, that the refractive index falls down from 2.6 for as deposited TiO_2 to 2.0 for a F

=0.075 J/cm^2 irradiation. This decrease in value of the refractive index is a characteristic of porous surface.[22]

At the lowest F, the film remains transparent. Slightly increasing F, the transparency of the film is reduced as already reported in Ref. 12. Increasing F further, the films present an opaque granular white structure. Finally, the irradiated film becomes darker with increasing F. This color modification of TiO_2 could be explained by a phenomenon of "light trap" by the porosity.[23]

C. AFM measurements

From SEM images and color modification, it can be deduced that the film morphology is altered by the irradiation process. As the surface properties (surface energy and wettability) play an important role in industrial applications and are correlated with the surface morphology, AFM is used to obtain information about the surface topography of the films. From these AFM images (Fig. 5), we deduce the evolution of the rms roughness (Fig. 6). The film becomes rougher after irradiation. Although the roughness fluctuates a lot, the global way is an upward trend. In addition, the surface granules possess different irregular shapes, sizes, and separations.

A consequence of the roughening of the surface is the modification of the specific surface area; for instance, if we consider a 2D configuration (Fig. 7), the initial film could be transformed in different morphology (two triangles) but with the same initial area. The border line of the film will be modified too, following the new profile. The consequence is to increase the length of the initial border line.

The evolution of the increase in specific surface area is displayed in Fig. 8. Taking care of the factors affecting AFM measurements,[24] we observe that the specific surface is consequently increased up to 50%–60% of the initial surface. For such a surface that involves light absorption and pollutant adsorption, the importance of a high specific surface area is more than evident. N. Negishi [9] reported that crystallization of a-TiO_2 in classic annealing treatment causes a dras-

(a)

(b)

FIG. 4. Top view SEM micrographs of the as deposited TiO_2 film and irradiated film with $F=0.15$ J/cm^2, (a) and (b), respectively.
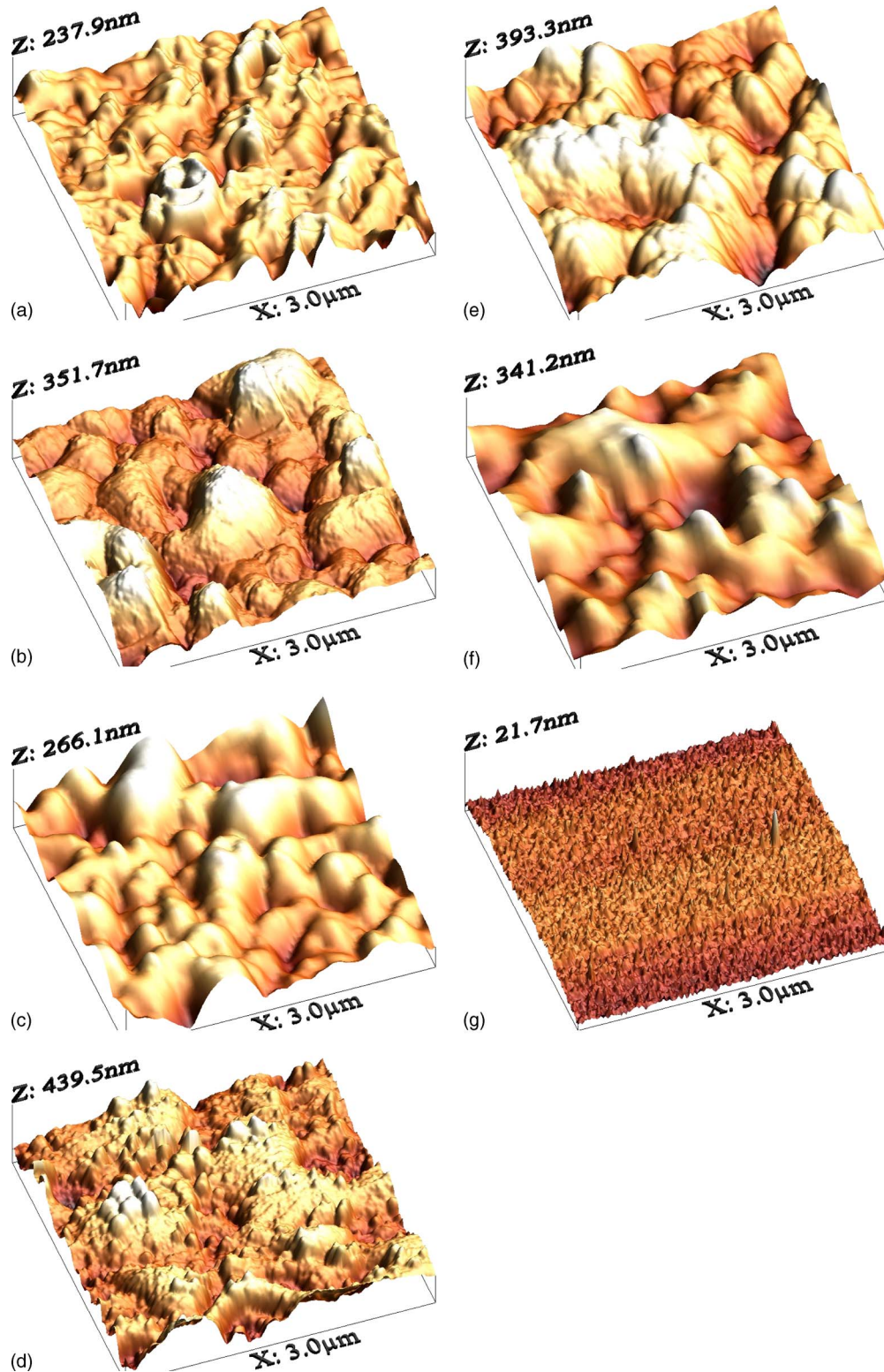
FIG. 6. (Color online) Evolution of the rms roughness of the film as a function of the laser fluence

tic decrease in the specific surface area. With excimer laser treatment, we create a-TiO$_2$ without losing the characteristic of higher specific surface area.

D. Contact angle measurements

One of the unique aspects of TiO$_2$ is that there are actually two distinct photoinduced phenomena: the well-known original photocatalytic phenomenon, which leads to the breakdown of organics, and the phenomenon called "super-hydrophilicity," which involves high wettability.[25] Even though there are intrinsically different processes, they can, and in fact, must, take place simultaneously on the same TiO$_2$ surface. Depending on the composition and the processing, the surface can have more photocatalytic character and less superhydrophilic character, or vice versa.[21]
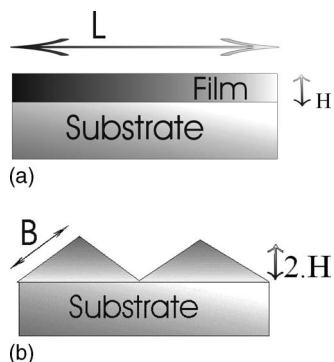
FIG. 7. Schematic 2D description of two different topographies with the same surface area.

FIG. 9. Evolution of the contact angle in the partial melting regime and in the melting-solidification regime.

In order to characterize the wettability of the surface, we performed contact angle measurements with a water drop on our surfaces. Figure 9 displays the evolution of the contact angle θ with F. It appears that θ increases in the range $0.075 < F < 0.1$ J/cm^2 and decreases linearly for $F > 0.1$ J/cm^2.

The contact angle of the nonirradiated film is equal to 87°. It falls down to 60° for the lowest fluence used here (0.075 J/cm^2 at which the surface has low roughness and good transparency). This is as expected since the a-TiO$_2$ phase surface is expected to be "wetting."[21] However, the increase and decrease in contact angle versus increasing and decreasing a-TiO$_2$ phase, respectively, gives us a negative feedback. This phenomenon leads us to suppose that except for the lowest fluence, the variations in contact angle are not related to the quantity of a-TiO$_2$. The roughness evolution could explain this behavior in the range of $0.075 < F < 0.1$ J/cm^2, as a rough surface is a nonwetting one. The nonwetting behavior is achieved, thanks to a high density spiky surface. Following AFM images, we could observe that the total topography results from the texturing of a relatively smooth large grain wavy surface by a large number of small peaks (Fig. 10). As we increase F, the small peaks disappear and let the large grain surface expand itself and drive the total topography. Therefore, for $F > 0.1$ J/cm^2 the
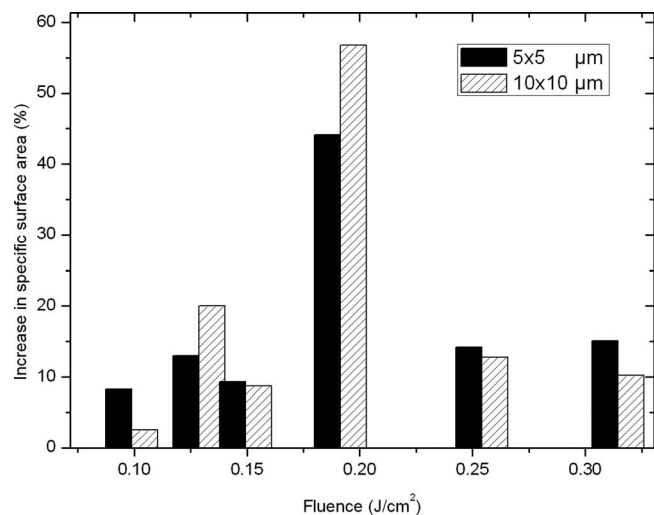
mean roughness is not varying a lot anymore, but the random repartition of large islands and valleys creates vacancies where the liquid could penetrate. The disappearance of the small peaks with increasing F could be due to their small size that could make them very sensitive to vaporization phenomenon.[14]

IV. DISCUSSION

A. Temperature calculation and nucleation

In order to understand the origin of the observed transformations, we have evaluated the temperature rise induced by the laser irradiation. We use a 2D model to study the heat transfer phenomena, which occur during the process. Using finite volume method analysis software FLUENT, the behavior of the induced surface temperature is studied as a function of F (Fig. 9). The thermal parameters used in the calculation are given in Tables I and II.[26–30]

It turns out that the melting temperature of TiO$_2$ is reached for $F \sim 0.13$ J cm^{-2}. This suggests that the strong increase in I_{101} occurring in the range $0.08 < F < 0.13$ J/cm^2 would take place via an amorphous to crystal

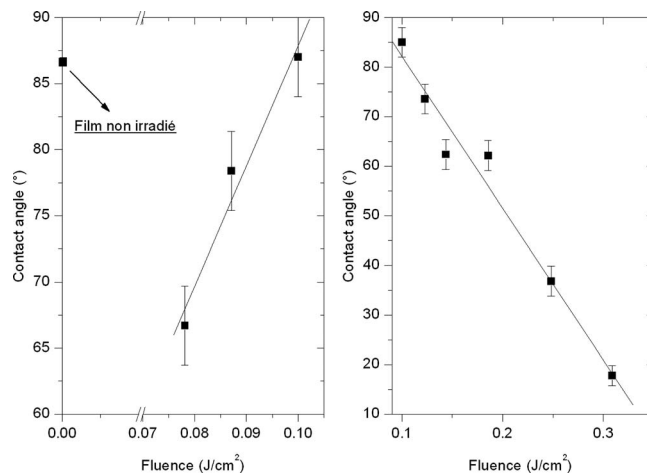FIG. 8. Ratio between the geometrically projected area and the area of the topography determined by AFM measurement.
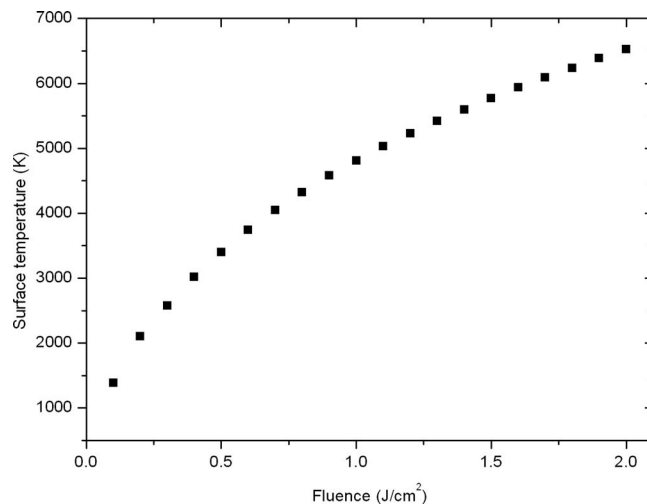

FIG. 10. Numerical simulation of the maximum induced surface temperature by means of FLUENT computational fluid dynamics software.

TABLE I. TiO$_2$ general properties used in temperature calculation.

	Density (kg/m^3)	Heat of melting (J/kg)	Molecular weight (kg)	Reciprocal light penetration depth (m^{-1})
TiO$_2$	3500	597 056	0.080	73 472 731
Glass	2510	146 440	0.060	100

nucleation process. The decrease in I_{101}, at $F > \sim 0.13$ J cm^{-2}, would result from a liquid to solid, i.e., a solidification, process. Although the nanosecond laser-solid interaction is a nonequilibrium process, the classical nucleation theory[31] could give some interesting information.

To crystallize the film it is necessary to overcome the nucleation barrier, which is given by[32]

$$\Delta G_c = (4f^3\gamma^3)/(27(G_2 - G_1)^2), \quad (1)$$

where f is a geometric factor, γ is the surface tension, and G_1 and G_2 are the energy for an atom in the phases 1 and 2 corresponding, in the present case, to amorphous and a-TiO$_2$. The probability to get nucleation depends on the probability to find a critical size nucleus. The number of such nuclei is given by

$$N^* = N \exp[(-\Delta G_c)/kT], \quad (2)$$

where N is the total number of atoms of the system, k is the Boltzmann constant, and T is the solidification temperature. N^* appears to be negligible when $(G_2 - G_1)$ is close to 0, but increases strongly for small values of $(G_2 - G_1)$. The strong increase in crystallization within small range of F, namely, between $F = 0.08$ J/cm^2 and $F = 0.13$ J/cm^2, could be associated with this explanation.

On the other hand, the maximum of crytallinity observed around $F = 0.13$ J/cm^2 (Fig. 1) could be explained by considering the crystallized TiO$_2$ volume fraction (I) produced by the irradiation treatment. Assuming spherical crystallites, the following equation can be written:[28]

$$I(T,t) = 4/3\pi n(T)v^3(T)t^4, \quad (3)$$

where t is the time, $n(T)$ the nucleation rate (related to N^*), and v the velocity of the interface between phases 1 and 2. The corresponding transformation-temperature-time diagram for crystallization of every crystal phase competing with glass formation is presented in Fig. 11. The bold line drawn on this diagram corresponds to the border between phase 1 (left side, amorphous TiO$_2$) and phase 2 (right side, a-TiO$_2$). This limit is often calculated for $I = 10^{-6}$.[27] Considering this curve and $t = 0$, the evolution of I as a function of T presents a maximum for a given T value. In our case, it corresponds

TABLE II. TiO$_2$ thermal parameters used in temperature calculation.

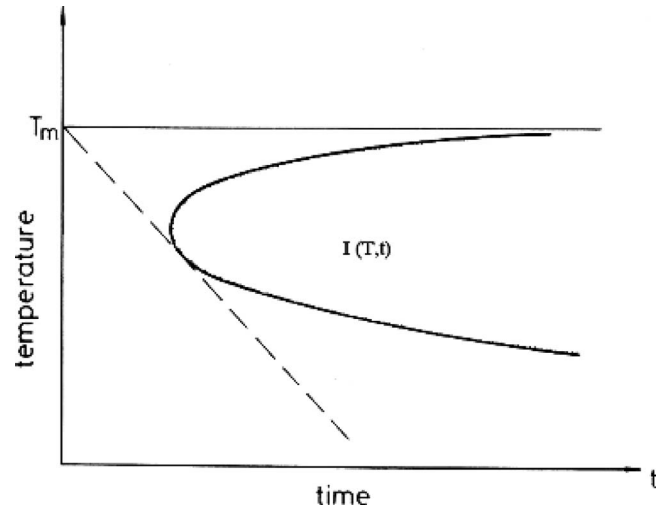|	Thermal diffusivity (m^2/s)	Thermal conductivity (W/m K)	Heat capacity (J/kg K)
TiO$_2$	$1.3 \cdot 10^{-6}$	3.5	$C_p = \{(-878)\exp[(-T)/165]\} + \{(-284)\exp[(-T)/2518]\} + 1119$
Glass	$5.2 \cdot 10^{-7}$		860

FIG. 11. Temperature, time, and transition diagram.

to a given F value which has been determined to be 0.13 J/cm^2.

Although the nucleation theory explains qualitatively the behavior of the crystalline fraction (the a-TiO$_2$ phase) with F, it disagrees quantitatively with the experimental results. Under thermal annealing, it is shown experimentally that, around 600 °C, it takes minutes to hours to obtain transformations.[8] In our cases, the transformations are in the 25 ns range, i.e., more than ten orders of magnitude quicker. The origin of this very large discrepancy is attributed to electronic effects. Indeed, the amorphous to crystal transition requires the rearrangement of covalent bonds. This can only be achieved via creation, migration, and recombination of dangling bonds sites,[33] which lead to a strong increase in the entropy of the transformation as well as to a strong decrease in the formation and migration energies of dangling bonds and hence to a significant increase in the crystal rate formation.

It has been argued that the effect of local electronic excitation around defects is to increase the entropy of the process (hence the pre-exponential factor) in Eq. (3). In order to meet the experimental data (an increase by a factor of 10^{10} of the pre-exponential factor), the corresponding entropy would have to increase by ΔS such that $\exp(\Delta S/k) \sim 10^{10}$, i.e., $\Delta S \sim 25k$. This is an unreasonably high value of ΔS. Therefore, although electronic effects might play a role, other mechanisms have to be considered, such as interface nucleation, stress effects, explosive crystallization, etc.

B. Surface morphology and fractal dimension

We mentioned above that the specific surface area is consequently increased as measured by AFM. Unfortunately, there is no method that yields the true surface area for microscopically rough surfaces.[20] In order to check the validity of our results by another way, we chose to investigate fractal dimension seeing that fractals are used to describe structures that exhibit the highly irregular behavior commonly found in nature.

Fractal geometry characterizes the scaling structure of a surface by a number $D_{fractal}$ called the fractal dimension that
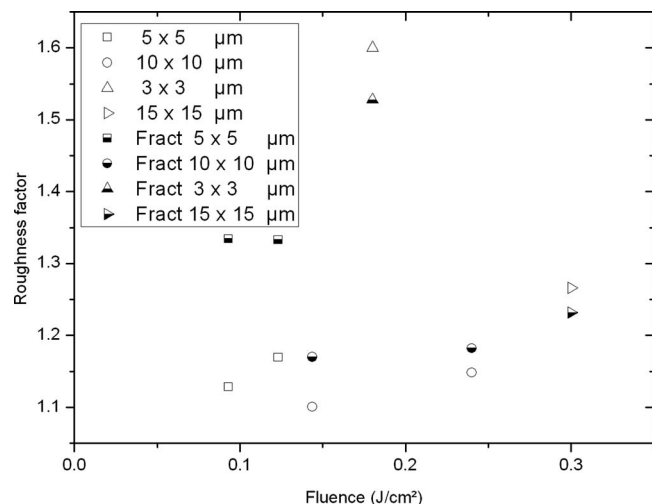
FIG. 12. Roughness factor comparison between classic and fractal methods.

varies between 2 (when the surface is flat) and 3.[34] The surface contains lakes within islands and islands within lakes, which we will refer to simply as islands. When the islands are characterized by a surface with a fractal dimension $D_{fractal}$, the coastlines formed by the islands sectioning by a plane are with a dimension $D'_{fractal} = D_{fractal} - 1$. The surface A of the island is linked to its radius R by the relationship $A \propto R^2$. The perimeter of the island P is linked to the fractal dimension of the thin film $D'_{fractal}$, with the relation $P \propto R^{D'_{fractal}}$. So the relationship linking the perimeter with the surface is a power law given by[34] $P = \mu A^{\alpha_{fractal}}$, where μ is the proportionality factor between the perimeter and the surface, $\alpha_{fractal} = D'_{fractal}/2$.

In order to characterize the surface topography by another way, we chose the *roughness factor r*, which is a useful dimensionless hybrid parameter defined by the relation

$$r = A_{film}/A_g, \tag{4}$$

where A_{film} is the area of the topography determined by any measurement technique and A_g is the geometrically projected area of the topography.

After irradiation, the surface area is increased and the effective surface extension of the film S_{film} could be related to the reduced fractal dimension by the relation[3]

$$S_{film} = (R_{film})^{D'_{fractal}}, \tag{5}$$

where R_{film} is the characteristic length of the scan area (for instance, if the AFM image is a 3×3 μm^2 one, $R_{film} = 3$ μm).

Thus, the roughness factor could be expressed by means of fractal theory assuming that $A_{film} = (S_{film} + A_g)$ and A_g is the scan area. From relations (4) and (5), it comes

$$r = [(R_{film})^{D'_{fractal}} + A_g]/A_g. \tag{6}$$

Figure 12 displays the evolution of the roughness factor, calculated by the fractal method [relation (6) with fractal dimension extracted by WSXM software] and by the classic method [relation (4) with A_{film} measured by WSXM]. This suggests that the fractal method and the classic one match quite well. The fractal method, which by definition is sup-

posed to be independent of the measurement resolution, confirms the specific surface characteristics obtained in Sec. III B. Moreover, the agreement between the results, obtained by relations (4) and (6), indicates that we created surfaces with high fractal comportment, as expected in Sec. III B. where we observed random distributions of islands and valleys.

V. CONCLUSIONS

TiO$_2$ thin films crystallized by single shot excimer laser irradiation at different laser fluences have been investigated by x-ray diffraction, SEM, AFM, Raman scattering, and contact angle measurements. Raman scattering shows that a-TiO$_2$ phase possesses better quality crystal in the partial melting regime ($0.075 < F < 0.13$ J/cm^2) than in the melting-solidification one ($F > 0.13$ J/cm^2). It can be seen by means of AFM and SEM imagery that the total morphology has been strongly modified by the process. The surface displays hydrophobic behavior comportment with increasing fluence in the $0.075 < F < 0.1$ J/cm^2 range and hydrophilic behavior for $F > 0.1$ J/cm^2, this last trend is associated with the evolution of roughness. This irradiation method could create high porosity surface with an increase in specific surface area for all fluences. However, pulsed laser annealing method could be considered as damaging one, at low enough laser fluence; the process could generate interesting combination of surface characteristics such as good transparency, anatase crystal structure, and low roughness porous surface with non-negligible specific surface area.

[1] T. Zhu, Y. P. Wang, L. Zhou, and Z. G. Liu, Mater. Sci. Eng., B **89**, 390 (2002).
[2] W. H. Ching M. Leung, and D. Y. C. Leung, Sol. Energy **77**, 129 (2004).
[3] A. P. Xagas, E. Androulaki, A. Hiskia, and P. Falaras, Thin Solid Films **357**, 173 (1999).
[4] Y. Choi, S. Yamamoto, T. Umebayashi, and M. Yoshikawa, Solid State Ionics **172**, 105 (2004).
[5] S. Konstantinidis, J. P. Dauchot, and M. Hecq, Thin Solid Films **515**, 1182 (2006).
[6] Z. W. Chen, J. K. L. Lai, and C. H. Shek, J. Phys. D **39**, 4544 (2006).
[7] Z. W. Chen, J. K. L. Lai, C. H. Shek, and H. D. Chen, Appl. Surf. Sci. **250**, 3 (2005).
[8] B. R. Sankapal, M. Ch. Lux-Steiner, and A. Ennaoui, Appl. Surf. Sci. **239**, 165 (2005).
[9] N. Negishi and K. Takeuchi, Mater. Lett. **38**, 150 (1999).
[10] H. Zhang and J. F. Banfield, J. Mater. Res. **15**, 437 (1999).
[11] L. Mariucci, A. Pecora, G. Fortunato, C. Spinella, and C. Bongiorno, Thin Solid Films **427**, 91 (2003).
[12] R. Ishihara, P. Ch. van der Wilt, B. D. van Dijk, A. Burtsev, J. W. Metselaar, and C. I. M. Beenakker, Thin Solid Films **427**, 77 (2003).
[13] Z. W. Chen, J. K. L. Lai, and C. H. Shek, Chem. Phys. Lett. **422**, 1 (2006).
[14] O. Van Overschelde, S. Dinu, G. Guisbiers, F. Monteverde, C. Nouvellon, and M. Wautelet, Appl. Surf. Sci. **252**, 4722 (2006).
[15] O. Van Overschelde, G. Guisbiers, and M. Wautelet, Appl. Surf. Sci. **253**, 7890 (2007).

[16]Z. W. Chen, J. K. L. Lai, and C. H. Shek, Phys. Lett. A **345**, 218 (2005).

[17]I. Horcas, R. Fernández, J. M. Gómez-Rodríguez, J. Colchero, J. Gómez-Herrero, and A. M. Baro, Rev. Sci. Instrum. **78**, 013705 (2007).

[18]D. Bauerle, *Laser Processing and Chemistry* (Springer, Berlin, 2000).

[19]O. Van Overschelde, R. Snyders, and M. Wautelet, Appl. Surf. Sci. **254**, 971 (2007).

[20]T. Tesfamichael, N. Motta, T. Bostrom, and J. M. Bell, Appl. Surf. Sci. **253**, 4853 (2007).

[21]S. Boukrouh, R. Bensaha, S. Bourgeois, E. Finot, and M. C. Marco de Lucas, Thin Solid Films **516**, 6353 (2008) .

[22]A. Verma and S. A. Agnihotry, Electrochim. Acta **52**, 2701 (2007).

[23]H. Y. Zheng, H. X. Qian, and W. Zhou, Appl. Surf. Sci. **254**, 2174 (2008).

[24]P. J. Ramon-Torregrosa, M. A. Rodríguez-Valverde, A. Amirfazli, and M. A. Cabrerizo-Vílchez, Colloids Surf. A Physicochem. Eng. Aspect. **323**, 83 (2008).

[25]M. Kaneko and I. Okura, *Photocatalysis Science and Technology* (Springer, Japan, 2002).

[26]J. F. Shackelford, *Materials Science and Engineering Handbook* (CRC, Boca Raton, 2001).

[27]D. R. Lide, *Handbook of Chemistry and Physics* (CRC, Boca Raton, 2007).

[28]W. Martienssen, *Condensed Matter and Materials Data* (Springer, New York, 2005).

[29]G. W. F. Drake, *Handbook of Atomic, Molecular and Optical Physics* (Springer, New York, 2006).

[30]W. W. Duley, CO_2 *Lasers Effects and Applications* (Academic, New York, 1976).

[31]M. von Allmen, *Laser-Beam Interactions with Materials* (Springer, Berlin, 1986).

[32]J. M. Poate and W. James, *Mayer, Laser Annealing of Semiconductors* (Academic, New York, 1982).

[33]M. Wautelet, P. Quenon, and A. Jadin, Semicond. Sci. Technol. **3**, 54 (1988).

[34]B. B. Mandelbrot, D. E. Passoja, and A. J. Paullay, Nature (London) **308**, 721 (1984).